

# Hard X-ray emission of the microquasar GX 339-4 in the low/hard state.

A. Joinet<sup>1</sup>, E. Jourdain<sup>1</sup>, J. Malzac<sup>1</sup>, J.P. Roques<sup>1</sup>, S. Corbel<sup>2</sup>, J. Rodriguez<sup>2</sup> and E. Kalemci<sup>3</sup>

## ABSTRACT

We present the analysis of the high energy emission of the Galactic black hole binary GX 339-4 in a low/hard state at the beginning of its 2004 outburst. The data from 273 ks of *INTEGRAL* observations, spread over 4 weeks, are analyzed, along with the existing simultaneous *RXTE* HEXTE and PCA data. During this period, the flux increases by a factor of  $\simeq 3$ , while the spectral shape is quite unchanged, at least up to 150 keV. The high energy data allows us to detect the presence of a high energy cut-off, generally related to thermal mechanisms, and to estimate the plasma parameters in the framework of the Comptonization models. We found an electron temperature of 60-70 keV, an optical depth around 2.5, with a rather low reflection factor (0.2-0.4). In the last observation, we detected a high energy excess above 200 keV with respect to thermal Comptonization while at lower energy, the spectrum is practically identical to the previous one, taken just 2 days before. This suggests that the low and high energy components have a different origin.

*Subject headings:* stars: individual: GX 339-4 - gamma rays : observations - black hole physics - accretion, accretion discs - X-rays : Binaries

## 1. Introduction

Since its discovery more than 30 years ago by Markert et al. (1973), the X-ray binary GX 339-4 has been extensively studied with several optical, infrared, X and  $\gamma$ -ray observatories. The optical companion is undetectable (Shahbaz, Fender and Charles 2001) but upper limits

---

<sup>1</sup>CESR/CNRS-UPS, 9 Avenue du Colonel Roche, BP4346, 31028 Toulouse, France

<sup>2</sup>Université Paris 7 Denis Diderot and Service d'Astrophysique, UMR AIM, CEA Saclay, F-91191 Gif sur Yvette, France.

<sup>3</sup>SabancıUniversity, Orhanlı- Tuzla, İstanbul, 34956, Turkey

on its luminosity allowed the source to be classified as a low mass X-ray binary which could belong to the Galactic bulge (with  $d_{min} \gtrsim 6.7$  kpc, Zdziarski et al. 2004). Hynes et al. (2003) propose to classify GX 339-4 as a black hole with a mass function of  $5.8 M_{\odot}$ .

The source harbours a complex variability behavior with a nearly persistent outbursting X and  $\gamma$ -ray activity and the presence of quite long periods of quiescence (Kong et al. 2002). In the soft X-rays it was observed at high-resolution with *Chandra* and *XMM* (Miller et al., 2004a, b) while Belloni et al. (2005) reports on the source timing and color analysis. At higher energy its emission has been studied by all the major observatories as *GRANAT* SIGMA (Grebenev et al. 1993, Bouchet et al. 1993), *CGRO* (Grabelsky et al. 1993). Zdziarski et al. (2004) present an extensive spectral analysis of the source covering the 1987-2004 period using *CGRO* BATSE, *GINGA* ASM and *RXTE* data. Homan et al. (2005) present a coordinated multi-wavelength study of the 2002 outburst and suggest a non-thermal/jet origin for the optical/near-infrared emission (Corbel & Fender 2002) in the hard state while the accretion disk dominates in the soft state.

In transient galactic black holes such as GX 339-4, the accretion rate varies by several orders of magnitude. They consequently exhibit a complex spectro-temporal variability. X-ray monitoring campaigns (with e.g. *RXTE*) demonstrated the existence of two main X-ray spectral states. Sources are usually observed with a X-ray luminosity lower than a few percents of the Eddington luminosity in the so called Low Hard State (hereafter LHS), characterised by a relatively low flux in the soft X-rays ( $\lesssim 1$  keV) and a high flux in the hard X-rays ( $\sim 100$  keV). In the LHS, the high-energy spectrum can be roughly described by a power-law with spectral index  $\gamma$  varying in the range 1.4-2.1, and a nearly exponential cut-off at a few hundred keV (see e.g. Gierliński et al. 1997). When the luminosity exceeds a few percents of Eddington the sources can switch to the High Soft State (HSS). The high-energy power-law is then much softer ( $\gamma \geq 2.4$ ), without any hint for a high energy cut-off and the bolometric luminosity is dominated by the disc thermal component peaking at a few keV. Beside the LHS and HSS, there are several other spectral states that often appear, but not always, when the source is about to switch from one of the two main states to the other. Those states are more complex and difficult to define. We refer the reader to McClintock & Remillard (2006) and Belloni et al. (2005) for two different spectral classifications based on X-ray temporal as well as spectral criteria and radio emission (Fender 2006). The hard power law plus cut-off spectrum of the LHS is usually interpreted as thermal comptonisation in a hot ( $kT_e \sim 100$  keV) optically thin plasma (the corona). In addition to the dominant comptonisation spectrum there are several other less prominent spectral features:

- a weak soft component associated to the thermal emission of a geometrically thin optically thick disk is occasionally detected below 1 keV as observed in Cygnus X-1 (Balucinska-Church et al. 1995) or in XTE J1118+480 (McClintock et al. 2001, Chaty

et al. 2003).

- a Fe  $K\alpha$  line at  $\sim 6.4$  keV and a Compton reflection bump peaking at  $\sim 30$  keV are believed to be the signature of the irradiation of the cold optically thick disc by the hard X-rays from the corona (George & Fabian 1991).
- a high energy ( $\geq 200$  keV) excess with respect to simple thermal Comptonization models was detected in GX-339-4 by OSSE (Johnson et al. 1993) during the LHS of its 1991 outburst. A similar excess was detected by COMPTEL in the LHS of Cygnus X-1 (McConnell et al. 2000). This excess is possibly produced by a tiny population of non-thermal electrons that could be, or not, part of the coronal plasma. With *INTEGRAL* SPI, we have the opportunity to monitor the excess above 200 keV which, as discussed in section 4, is crucial to address the emission mechanism at these energies.

In this paper, we will focus only on observations performed when GX 339-4 was in the LHS, while Belloni et al. (2006) study the evolution of the high energy cutoff during the transition from the low/hard to the high/soft state. We will present here the overall available *INTEGRAL* SPI+IBIS and simultaneous *RXTE* PCA+HEXTE data (see Table 1) which cover the rising phase of the 2004 outburst.

The analysis is based on the data registered from MJD 53057 (*INTEGRAL* revolution 166 on 2004 February 4) to MJD 53085 (*INTEGRAL* revolution 175 on 2004 March 21) limiting us to the low/hard state study.

We will briefly describe the *INTEGRAL* and *RXTE* telescopes as well as data analysis methods in Section 2.

The results, which concern mainly spectral evolution, are presented in Section 3, then discussed in Section 4.

## 2. Observations and data analysis

The first indication of a new reactivation of GX 339-4 has been provided by Buxton et al. (2004) who reported a radio and optical source fluxes increase on 2004 February 4-5. Then on 2004 February 9, the X-ray activity has definitively renewed (Smith et al. 2004, Belloni et al. 2004) and the source was detected by *INTEGRAL* on 2004 February 19 (MJD 53054) (Kuulkers et al. 2004). This paper is based on data taken during the first part of the outburst when the source was in the hard state. Table 1 gives the details of each *INTEGRAL* revolution and corresponding quasi simultaneous *RXTE* observations used in this analysis

(i.e. for the LHS). Figure 1 shows the *RXTE* ASM light curve of the source in the 1.5-12 keV energy range together with *INTEGRAL* observation periods.

## 2.1. *INTEGRAL*

### 2.1.1. *SPI*

*SPI* (Spectrometer for *INTEGRAL*, Vedrenne et al. 2003, Roques et al. 2003) is one of *INTEGRAL*'s two main instruments. Working in the 20 keV - 8 MeV energy domain with 19 hexagonal germanium detectors, it possesses an excellent energy resolution and a  $16^\circ$  (corner to corner) field of view.

*SPI*'s imaging capability is limited with a  $2.5^\circ$  angular resolution using a HURA (Hexagonal Uniform Redundant Array) coded mask, whose cells have the same size as the individual detectors. Due to the small number of detectors (pixels), *SPI* image reconstruction methods are based on a combination of data from several pointings separated by  $2^\circ$  and covering the same sky region ("dithering strategy", see Jensen et al. 2003).

During the  $\simeq 3$  day *INTEGRAL* revolution, the observing schedule consists of fixed pointings lasting approximatively 30-40 minutes, with a complete dithering pattern made up of 25 pointings (in  $5 \times 5$  rectangular mode, except during the observation program of the GCDE where the pattern is specific) separated by a  $2^\circ$  angular distance. This method increases the amount of data in excess of the number of unknowns, and allows to better determine the background and the position and the flux of sources on the detector plane.

The signal recorded by the *SPI* camera on the 19 Ge detectors is composed of the contributions from each source in the field of view through the instrument aperture, plus the background, which comes mainly from the interaction of high energy particles ( from cosmic rays or due to solar activity) with the instrument.

For  $N_s$  sources present in the field of view, the data  $D_p$  obtained during a pointing  $p$  for a given energy band can be expressed by the relation:

$$D_p = \sum_{i=1}^{N_s} R_{p,i} \otimes S_{p,i} + B_p \quad (1)$$

where  $R_{p,i}$  is the response of the instrument for the source  $i$ ,  $S_{p,i}$  the flux of the source  $i$  and  $B_p$  the background, recorded during the pointing  $p$ .  $D_p$  and  $B_p$  are vectors of 19 elements.

In the present work, we describe the background as  $B_p = A_p U$  where  $A_p$  is the normalisation coefficient per pointing and  $U$  the "uniformity map" of the SPI camera, derived from an empty field observation. The system consists of  $N_d$  (number of detectors)  $\times$   $N_p$  (number of pointings) equations solved simultaneously by a chi-squared minimisation method. The number of unknowns (free parameters) is  $N_p \times (N_s + 1)$  (for the  $N_s$  sources and the background fluxes) but we can reduce them by realising that the time variability for the sources and the background is longer than a single pointing.

The timescales depend on the goal of the analysis. For the image reconstruction performed by the SPIROS detection algorithm (Skinner & Connell 2003), source and background fluxes are generally assumed to be constant during the whole set of observations. In SPIROS, the source positions are extracted using an iterative source research technique, implemented for the coded mask telescope *INTEGRAL* SPI. The fluxes determined in this way are thus rough mean fluxes, the main goal being to extract source positions.

To build the light curves of the sources detected in the field of view, we must choose the appropriate time scale for each component (sources and background). Concerning the background flux, the global count-rates registered with the Anti-Coincidence System (ACS) indicate that the background flux is stable within each of the considered revolutions. For the sources, it is important not to oversample the temporal variability as this increases the errors and provides no further scientific information. We have chosen a time scale for each source mainly as a function of its intensity, and of its a priori known or observed temporal behavior. The fainter sources have been considered to have a constant flux within a revolution. For the brightest sources, we test several values and choose the longest timescale over which the source is found not to vary (see below). The system of  $N_d \times N_p$  equations (1) is thus completed by a number of additional constraints reflecting the non-variability of a given parameter ( $S_{p,i}$  for a source or  $A_p$  for background) over its timescale ( $\Delta t_i$ ). The resolution of this system by the chi-squared minimisation method gives the light curves of all components simultaneously.

The count spectra are constructed by solving a similar set of equations in a number of energy bands, and then deconvolved using the energy response matrix corresponding to each pointing (Sturmer et al. 2003) to get the photon spectra. We added a 3% systematic error to all spectral channels, and the spectra were fitted from 23 to 600 keV in XSPEC.

Only pointings for which GX 339-4 was at a distance lower than 12 degrees from the central axis were taken into account for the analysis. We excluded pointings affected by a solar flare or by exit/entry into the radiation belts. We obtained 273 ks of useful data with 140 pointings during the observation period covered by the revolutions 166, 167, 174 and 175 (see Table 1).

### 2.1.2. *IBIS*

The Imager On Board *INTEGRAL* (IBIS) is a coded mask telescope with a total field of view of  $29^\circ \times 29^\circ$  (down to 0 response) composed of a two layers detection plane. We use here only data from the upper layer, the *INTEGRAL* Soft Gamma-Ray Imager (ISGRI, Lebrun et al. 2003). This detector is sensitive from  $\sim 13$  keV to about 1000 keV.

Due to its low efficiency and the general faintness of the fluxes of sources above  $\sim 400$  keV, it has generally a limited use above that energy.

IBIS/ISGRI has excellent imaging capabilities with an angular resolution of  $12'$  and a positional accuracy around  $1'$  depending on a given source signal to noise ratio. ISGRI also possesses spectral capabilities, although with a much poorer resolution than SPI, with  $\Delta E/E \sim 0.1$  at 60 keV.

The data from IBIS/ISGRI were reduced in a manner strictly identical to the one reported in Rodriguez et al. (2006) which focuses on the same field with the exception that the last version of the Offline Scientific Analysis (OSA) software (V 5.1) was used. To quickly summarize, we first produced images in 2 energy ranges (20-40 keV, and 40-80 keV), to identify the most active sources. We then extracted spectra from all the sources in this field that had a detection significance higher than 7. We rebinned the original response matrix (`isgri_rmf_grp_0016.fits`) to 63 channels before the extraction. The latest time dependent ancillary response file (`isgri_arf_rsp_0013.fits`) was then associated to the file for the spectral fits. We added 2% systematics to all spectral channels, and the spectra were fitted (together with those from the other instruments) from 25 to 200 keV.

## 2.2. *RXTE*

We also analysed the public PCA+HEXTE (Bradt et al. 1993, Rothschild et al. 1998) data. Table 1 summarizes the set of *RXTE* observations performed contemporaneously with the *INTEGRAL* data observation periods.

We limited the energy range from 3 to 25 keV, and 25 to 200 keV for the PCA and HEXTE data respectively. The data reduction was done using the FTOOLS routines in the HEASoft software package distributed by NASA's HEASARC (version 5.2). We followed the steps of standard reduction as explained in the *RXTE* Cook Book. The spectrum extraction was performed from data taken in "Standard 2" mode. The response matrix and the background spectra were created using FTOOLS programs. Background spectra were made using the latest "bright source" background model.

Only the proportional counter unit (PCU) number 2 of the PCA (Bradt et al. 1993) detector has been used for the data extraction. We added 0.8% up to 7 keV and 0.4% above 7 keV as systematic error (for the details of how we estimated systematic uncertainties, see Tomsick et al. 2001).

For HEXTE, we used the response matrix created by the FTOOLS, and applied the necessary dead time correction (Rothschild et al. 1998). The HEXTE background is measured throughout the observation by alternating between the source and background fields every 32 s. The data from the background regions are merged. HEXTE channels were grouped by 2 for channels 16-31, by 4 for channels 32-59, by 10 for channels 60-99 and by 64 for channels 100-227.

By fitting HEXTE data during the observation period of revolution 175 with a power-law plus cutoff model, we found a  $\chi^2$  value of 2.15 (12 dof). All the fits including these HEXTE points are clearly degraded. Therefore we suspect a problem for this particular data set (see  $\chi^2$  values in tables 4, 5 and 6). Thus we decided for this particular revolution, to perform the analysis with and without the HEXTE data. We stress that including the HEXTE data vastly degrades the  $\chi^2$ , thus we don't consider the corresponding results in the discussion.

### 3. Results

#### 3.1. Field of view around GX 339-4: flux extraction

Several hard X-ray sources are present in the GX 339-4 field and have to be carefully taken into account with appropriate variability time scales in the SPI analysis.

The sources detected above 20 keV using SPIROS, for revolutions 166 + 167, are listed with their 23-50 keV mean fluxes in Table 2.

As mentioned in Section 2.1, the errors increase with the number of sources and temporal bins. So we make sure that each additional degree of freedom really improves the  $\chi^2$ . First, due to its highly variable behavior, the 4U1700-377 light curve in the 23-200 keV energy range requires the use of the highest timescale resolution, ie one pointing (whose duration is about 1770 s during revolution 166, 2700 s for the others). Then timescale variabilities of a 3 (for 4U 1630-47, GX 354-0 and GX 340+0) and 2 (for OAO 1657-415) pointings duration were found to significantly improve the  $\chi^2$ . We consider finally 6, 4 and 2 other sources, including GX 339-4, with a constant flux for revolutions 166+167, 174 and 175 respectively. The resulting 23-44 and 44-95 keV fluxes obtained with SPI for GX 339-4 are presented in

Table 3. The quoted errors are at  $1\sigma$  level. It appears that the source flux increases by a factor 3 between revolutions 166+167 and revolutions 174 and 175.

When going to higher energies, the sources significances decrease (see Table 2) and we thus consider only 5 sources to extract fluxes above 150 keV.

### 3.2. Spectral evolution

The GX 339-4 spectra corresponding to each set of data detailed in Table 1 have been fitted with various models available in the standard XSPEC 11.3.1 fitting package (Arnaud 1996). In all cases, we account for the interstellar absorption (PHABS in XSPEC) using a column density  $N_H$  of  $3.7 \times 10^{21} \text{ cm}^{-2}$  (Miller et al. 2006). In all fits, the iron emission line was modelled by a narrow Gaussian fixed at an energy of 6.4 keV. As the width of the line is only weakly constrained it was fixed at 0.1 keV. For all models, the inner disk inclination was fixed at  $50^\circ$ . The data of revolutions 166 and 167 have been added to improve statistics, due to the low flux of the source and short duration of the revolution 167.

We used the simultaneous PCA (3-25 keV), HEXTE (25-200 keV), IBIS (25-200 keV) and SPI (23-600 keV) data for the spectral analysis.

#### 3.2.1. PEXRAV model

First, we fitted all data with the PEXRAV model (Magdziarz & Zdziarski 1995) consisting of a power-law with a high energy cut-off and reflection from neutral medium.

Fixing the reflection fraction to  $\Omega = 0$  provides a marginally acceptable fit for revolution 166+167 (reduced  $\chi^2$  of 1.11) and a very poor description of the data for revolutions 174 and 175 (reduced  $\chi^2$  of 2.12 and 2.86 respectively). The pattern of residuals is characteristic of the presence of Compton reflection. Adding a reflection component improves the fit dramatically, reducing the  $\chi^2$  to 0.82, 0.91 and 1.09 for revolutions 166+167, 174 and 175 respectively (see Table 4).

The addition of a Compton reflection gives a better fit at a high significance during all those observations, with a probability  $\lesssim 10^{-13}$  that adding this component is not required by the data (as obtained using the F-test).

We see in Table 4 that the reflection fraction increases and reaches a value of  $\sim 0.5$  when the flux is high. The photon index is around 1.6-1.7 as usually observed, but the energy cut-off is rather high (300-400 keV). To test the reality of the cut-off, we perform fits



with the same model but fixing  $E_c$  to 2 MeV (i.e. outside our energy range). The fit with a free high energy cut-off is significantly better in all cases with F-test probability of  $10^{-12}$ ,  $3 \times 10^{-17}$  and  $2 \times 10^{-12}$  for revolutions 166+167, 174 and 175 respectively. We attempted to fit with ionized reflection using the PEXRIV model but the best fit ionization parameter tends to zero.

### 3.2.2. Physical models based on Comptonization

To go more deeply into the understanding of the source behavior, we have used more sophisticated models, based on the Comptonization process as it is thought to be the main mechanism able to produce the emission observed in our energy domain.

#### *COMPPS model*

First, we modelled the X- and  $\gamma$ -ray spectrum with the thermal Comptonization model COMPPS (Poutanen & Svensson 1996). Blackbody seed photons are injected into a spherical corona of uniform optical depth  $\tau$ , and temperature  $kT$  where they are Comptonized. The temperature of the blackbody component cannot be constrained and was frozen to 390 eV (Miller et al. 2006).

A fraction of the hard X-rays is scattered back into the disk where it is reflected. We consider the case of reflection from cold, neutral material with solar abundances.

As seen from Table 5, the temperature and the optical depth can be considered as constant as well as the equivalent width which was found to a value of about 90 eV. Only the reflection fraction varies, increasing from 0.2 up to 0.4, between the first (low intensity) and the 2 last observations (brighter by a factor of 3).

We see from Figure 2 that the global shape of the spectrum is unchanged between observations 174 and 175 as well as the flux of the source (see Table 5). But in the latter, an excess of emission relatively to the model appears above 200 keV. This is unexpected from thermal model and we thus investigated this point more deeply.

We first reconstructed the image in the 200-437 keV energy band for both revolutions 174 and 175 (Figure 3). While the image of revolution 174 doesn't reveal any significant feature, the highest excess detected by SPIROS for revolution 175 coincides with the GX 339 position. Note that the distribution and the level of the residuals in both images follow the expected ones, thus allowing to be confident in the data reduction process. We can assess

that all statistical tests show a low level of systematics. Thus the measured significance of the emission ( $4.6 \sigma$ ) has not to be corrected.

Figure 4 presents the high energy part of the source spectrum for revolutions 174 and 175, while in Figure 5 are displayed the data for all instruments, together with the corresponding residuals relatively to the COMPPS model. They show that SPI and IBIS data are in agreement even if the IBIS points above 200 keV are not significant. The IBIS measurement in the 200-437 keV energy band gives an  $3\sigma$  upper limit of 223 mCrab, to compare to the SPI measurement of  $218 (\pm 47)$  mCrab.

We have thus used only the SPI data to quantify this excess relatively to the thermal emission. The shape of the SPI spectrum during the revolution 175 has been fitted using the COMPPS model. The best fit parameters are an electron temperature kT of 44 keV and an optical depth of 4.4 (with a reduced  $\chi^2$  of 1.35). We found that the addition of a simple power-law leads to an improvement of the fit of the SPI data significant at the 90 % level according to a F-test, with a best fit photon index of 1.07.

### *EQPAIR model*

We finally applied the hybrid thermal/nonthermal Comptonization model EQPAIR (Coppi, 1999). This model assumes a spherical plasma cloud with isotropic and homogeneous distribution of electrons, positrons and soft seed photons within the plasma. The properties of the plasma depend on its compactness  $l = L\sigma_T/Rm_e c^3$ .  $L$  is the power of the source,  $R$  the radius of the sphere which is assumed to be  $10^7$  cm and  $\sigma_T$  is the Thomson cross-section. We use a hard compactness  $l_h$  which corresponds to the power supplied to the electrons, and a soft compactness  $l_s$ , corresponding to the power supplied in the form of soft seed photons. The amount of heating of the Comptonizing medium is specified through the ratio of the compactnesses of the Comptonizing medium  $l_h$ , and of the seed photon distribution  $l_h/l_s$  with  $l_s$  fixed to 1. The seed photon blackbody temperature  $kT_{seed}$  is frozen to 390 eV. The reflection component is modelled as in COMPPS and the reflection fraction  $\Omega/2\pi$  obtained from the fit corresponds to the unscattered part of the Compton reflection component. The total optical depth, ( $\tau_{tot}$ ), is the sum of the optical depth of  $e^+e^-$  pairs ( $\tau_{e^+e^-}$ ), and of  $e^-$  coming from ionization of atoms ( $\tau_{es}$ ). The fitted parameters are  $l_h/l_s$  (which is related to the coronal temperature) and the ionization electron optical depth,  $\tau_{es}$ .

In order to consider the case of a hybrid plasma, the model contains an additional parameter: the ratio  $l_{nth}/l_{th}$  where  $l_{nth}$  is the compactness corresponding to the non-thermal and  $l_{th}$  to the thermal part of the  $e^+e^-$  distribution. The rate at which non-thermal electrons appear in the source is assumed to be a power-law,  $\gamma^{-\Gamma_{inj}}$  between the Lorentz factor  $\gamma_{min} = 1.3$

and  $\gamma_{max} = 1000$ .  $\Gamma_{inj}$  is assumed to be equal to 2. We combined EQPAIR with a gaussian iron line centered and fixed at 6.4 keV with a width of 0.1 keV. Table 6 shows the evolution of the best fit parameters.

We first fixed the compactness of the non-thermal electrons to zero in order to consider the case of a purely thermal plasma. Spectra extracted during all the observations are well fitted with  $\chi^2 \simeq 0.8 - 1.1$ . The hard-to-soft compactness ratio is in the range of 5-6 yielding a coronal temperature of about 65 keV, given the fitted optical depth of 1.6 in revolutions 174-175 while the kT (98 keV) and  $\tau_{tot}$  (1.1) parameters of revolutions 166+167 are very different. Part of the difference between the kT and  $\tau$  best fit values can be explained by the fact that the Comptonization model suffers from a degeneracy in their determination due to low statistic. Indeed the spectral slope depends only on the Compton parameter  $y = 4 \times kT \times \tau / m_e c^2$  which does not vary a lot along the observations (see Table 6). In fact, if we freeze the optical depth in revolution 166+167 to the value obtained in revolution 174 we obtain an acceptable  $\chi^2$  value and the difference in temperature between both revolutions decreases. Nevertheless the  $y$  parameter seems to be larger in revolution 166+167 which is confirmed by a significantly higher  $l_h/l_s$ .

The reflection component fraction is similar to the value found with COMPPS model and the iron line equivalent widths are still about 90 eV.

In a second step, the compactness of the non-thermal distribution has been freed in order to consider the case of an hybrid plasma.

For revolution 174, this leads to a thicker ( $\tau_{tot} \simeq 2.0$ ) and cooler ( $kT_e \simeq 50$  keV) solution, relatively to the thermal case, with both solutions equivalent from a statistical point of view.

Moreover, determining the confidence range of the  $l_{nth}/l_{th}$  parameter, we found it unconstrained, forbidding any conclusion.

The situation seems different for the revolution 175 as the introduction of a non-thermal component allows a slight improvement of the  $\chi^2$  (with a FTEST probability of  $10^{-2}$ ) even though the non-thermal fraction is not really constrained. However, the parameters are the same as in the thermal case except the hard compactness which slightly increases.

## 4. Discussion

### 4.1. Comparison with previous observations

Broadband X and  $\gamma$ -ray spectrum of GX 339-4 using data collected from SPI, IBIS, HEXTE and PCA instruments allowed us to follow the source behavior during the low/hard

state corresponding to the rising phase of its 2004 outburst. During this period we observed a flux increase by a factor 3 in the whole energy domain (3 - 200 keV) without any major change in the spectral shape (see Figure 2). This is similar to results from previous outbursts reported by Zdziarski et al. (2004, Figure 4) where, during the LHS, in the rising phase, the source flux increases at constant spectral slope.

#### 4.1.1. High energy cut-off and the reflection component

We showed that reflector and high energy cutoff in the primary emission component were required to describe the spectral shape during the LHS, as typically observed for GX 339-4. Simultaneous fits from PCA, HEXTE, IBIS and SPI data give photon indexes  $\Gamma$  in the range of 1.6-1.7 with cut-off energies around 300-400 keV. The amplitude of the reflection component reaches similar values to those reported by Revnivtsev et al. (2001), who modelled the low/hard state of GX 339-4 during its outbursts of 1996-1997 as observed by PCA. They found photon indexes  $\Gamma$  in the range of 1.7-1.9 and a reflection amplitude of 0.3-0.5. Moreover the reflection fraction increases with the photon index of the power-law and flux in a way similar to the correlation already observed by Nowak et al. (2002) for GX 339-4 and in a large sample of Seyfert and X-ray binaries by Zdziarski et al. (1999, 2003). Zdziarski et al. (1999) have interpreted the  $\Omega$ - $\Gamma$  correlation as being due to feedback in an inner hot (thermal) accretion flow surrounded by an overlapping cold disc. Then, the closer to the central black hole the cold disc extends, the more cooling of the hot plasma by blackbody photons (indicated by the decrease of the electron temperature  $kT$  fitted by the COMPPS model) and the softer the spectrum (as shown from the powerlaw slope  $\Gamma$  fitted by PEXRAV model).

#### 4.1.2. Comptonization parameters

We then introduced the physical models COMPPS and EQPAIR to describe the GX 339-4 observations with Comptonization process. From a statistical point of view, both models give acceptable solutions. Data from revolutions 166+167 and 174 are well fitted with Comptonization model in a purely thermal case, while the last revolution suggests the presence of a non-thermal component.

Wardzinski et al. (2002) modelled the outburst of September 1991 observed by Ginga/LAC and CGRO/OSSE as well as the outbursts of 1996 and 1997 observed by *RXTE* PCA+HEXTE with COMPPS model. The Comptonization spectrum was characterised by Thomson opti-

cal depths  $\tau$  of 2.4-3.0 and electron temperature of 60 keV. The reflection component was found to be moderately ionized with amplitudes ranging from 0.2 to 0.4. We have tested the ionized case, but the ionization parameter tends to zero. We have thus fixed it to zero and in fact deduced very similar best fit parameters.

The EQPAIR thermal model has been used by Nowak et al. (2002) to interpret the spectra obtained during the low/hard state observations of the GX 339-4 outbursts in 1997 and 1999 by PCA+HEXTE. With a fitted seed photon temperature of 30-100 eV, they found coronal compactnesses  $l_c$  ranging from 5 to 14 and electron optical depths  $\tau_{es}$  from 0.01 to 0.6, yielding to total optical depths  $\tau_{tot}$  between 0.1 and 1 and  $kT_e$  around 200 keV. The reflection fractions are between 0.1-0.5 and the equivalent widths of the iron line range from 80 to 240 eV. We find similar values for the reflection fraction, iron line width and coronal compactness, but thicker ( $\tau_{tot}$  around 1.6-1.7) and colder ( $kT_e$  around 65 keV) plasma parameters.

#### 4.2. The high energy excess

An interesting feature appears in the SPI data at revolution 175 as the emission extends beyond the thermal cut-off. Such an excess above 200 keV has already been observed by the OSSE observatory (Johnson et al. 1993) in the low/hard state of the GX 339-4 outburst event in September 1991. Assuming a distance of 6 kpc, the luminosity above 200 keV was  $11.3 \times 10^{36}$  erg s<sup>-1</sup> (Johnson et al. 1993) with a 35-300 keV luminosity  $L_{35-300 \text{ keV}}$  of  $2.5 \times 10^{37}$  erg s<sup>-1</sup>. These values are comparable to what we found for the excess observed during revolution 175 with a luminosity above 200 keV of  $7.2 \pm 1.6 \times 10^{36}$  erg s<sup>-1</sup> and  $L_{35-300 \text{ keV}} \simeq 1.54 \times 10^{37}$  erg s<sup>-1</sup>. More recently, a similar feature has been reported in one *RXTE* observation (Nowak et al. 2002), where the HEXTE spectrum exhibits a hardening above  $\sim 100$  keV.

Similar behavior is observed for Galactic black hole transients in the LHS during the ourburst decays, especially after the detection of compact jets (Kalemci et al. 2006; Kalemci et al. 2005).

The flux extension above a thermal Comptonization component can be explained by a second Comptonization region/population or, more or less equivalently, spatial (gradient) and/or temporal variations in the plasma parameters. As our fitting models assume them to be homogeneous and constant during one observation, such variations can produce deviation relatively to the predicted spectrum. Another possibility could be the presence of a large annihilation line which would produce a bump extending down to 250-300 keV. Alternatively, some models include the presence of a non-thermal electron population in the plasma.

The high energy power-law tail observed for Cyg X-1 in its LHS has been modelled with a hybrid Comptonization, by injecting an electron population consisting of Maxwellian distribution coupled to a power-law with an index of 4.5 (McConnell et al. 2000). The presence of a high-energy electron tail has also been proposed by Wardzinski et al. (2002) for GX 339-4 simultaneous observations of PCA+HEXTE and CGRO/OSSE during the outburst of 1997, even though COMPSS model fits the data reasonably well. They found that the introduction of a non-thermal fraction of electrons improves the  $\chi^2$ , and corresponds to 34 % of non-thermal emission.

The EQPAIR hybrid plasma allows a marginally better description of the spectrum during revolution 175. Adding a non-thermal parameter  $l_{nth}$  to the pure thermal plasma case gives an FTEST value of about  $10^{-2}$ . However, the  $l_{nth}/l_{th}$  fraction ( $\simeq 0.28$ ) is similar to the value found for the LHS of GX 339-4 by Wardzinski et al. (2002), even though these values are in fact not constrained.

In Galactic black holes, non-thermal emission is generally associated with the soft state (Grove 1999, Ling et al. 1994) or state transitions (see eg. Cadolle-Bel et al. 2006, Malzac et al. 2006), where power-law tails are observed, and attributed to Comptonization of soft photons by accelerated electrons. During the transition from the low/hard to the high/soft state on August 15 2003, Belloni et al. (2006) observed that the high energy cut-off increases/disappears.

In the LHS, the hard X/ $\gamma$  ray emission comes from a thermalised electron population. The presence in the low/hard state of a significant non-thermal emission above the thermal cut-off can however be interpreted in terms of an additional component. Contrary to the soft state where power-law tails are commonly observed, this characteristic is much rarer in the LHS. In our observations, this feature is detected only in one revolution, nevertheless the statistic is not high enough to conclude on its variability. Moreover, as the low energy part of the spectrum is not affected (the spectral shape is similar up to  $\simeq 150$  keV in revolutions 174 and 175), this may suggest that the involved phenomenon varies independently of the thermal Comptonization process and could come from another location such as jets or active regions. Jet can easily produce hard X-ray emission via synchrotron radiation in addition to inverse Compton up-scattering (see e.g. Markoff et al. 2003).

## 5. Conclusions

We investigated the high energy spectral characteristics of GX 339-4 in the low/hard state (rising phase of the outburst), using observations from *INTEGRAL* SPI+IBIS and

*RXTE* PCA+HEXTE. The plasma parameters deduced from thermal Comptonization models are identical to those obtained during previous observations performed when the source was in a similar spectral state, with a plasma temperature  $kT$  around 65 keV, an optical depth  $\tau \simeq 1.5 - 2.5$  and a reflection factor lower than 1 (0.2 - 0.4), supporting an anisotropic primary emission or a large value of the disk internal radius. An emission in excess relatively to the thermal cutoff has been detected during one revolution, while absent 3 days before. The corresponding flux (typically emission above 200 keV) is not highly significant with only  $4.6 \sigma$ , but can be compared to features reported by OSSE/CGRO and HEXTE in GX 339-4 or Cyg X-1. This can be an evidence that an additional component is sometimes present in the spectrum, unless variabilities (spatial and/or temporal) of ( $kT$ ,  $\tau$ ) plasma parameters can mimic such spectral evolution affecting only the energy domain above 200 keV.

The SPI project has been completed under the responsibility and leadership of the CNES. We are grateful to ASI, CEA, DLR, ESA, INTA, NASA and OSTC for support. Specific softwares used for this work have been developed by L. Bouchet. E. K. acknowledges partial support of TUBITAK and Marie Curie International Reintegration Grant MIRG-CT-2005-017203. The authors are grateful to the anonymous referee for its very fruitful comments that allowed us to improve the quality of this paper.

## REFERENCES

- Arnaud K. A. 1996, in ASP Conf. Ser., Vol. 101, Astronomical Data Analysis Software and Systems V, ed. G. H. Jacoby, J. Barnes J. (San Francisco: ASP), 17
- Baluncinska-Church, M., Belloni, T., Church, M. J., & Hasinger, G., 1995, *A&A*, 302, L5
- Belloni T., Homan J., Cui W., & Swank J., 2004, *Astron. Telegram*, 236
- Belloni, T., Homan, J., Casella, P., van der Klis, M., Nespoli, E., Lewin, W. H. G., Miller, J. M. & Méndez, M. 2005, *A&A*, 440, 207
- Belloni, T., et al. 2006, *MNRAS*, 367, 1113
- Bouchet, L., et al. 1993, *ApJ*, 407, 739
- Bradt, H.V., Rothschild, R.E., & Swank, J.K. 1993, *A&AS*, 97, 355
- Buxton, M., Gallo, E., Fender, R., & Bailyn, C. 2004, *Astron. Tel.*, 230
- Cadolle Bel, M., et al. 2006, *A&A*, 446, 591

- Chaty, S., Haswell, C. A., Malzac, J., Hynes, R. I., Shrader, C. R., & Cui, W., 2003, MNRAS, 346, 689
- Coppi, P. S. 1999, in ASP Conf. Ser. 161, High Energy Processes in Accreting Black Hole, ed. J. Poutanen & R. Svensson. (San Francisco: ASP), 375
- Corbel, S., & Fender, R. P., 2002, ApJ, 573, 35
- Fender, R.P., 2006, in Compact Stellar X-ray Sources, ed. W.H.G. Lewin & M. van der Klis (Cambridge: Cambridge University Press), p 381 astro-ph/0303339.
- George I.M., & Fabian A.C. 1991, MNRAS, 249, 352
- Gierliński, M., Zdziarski, A., A., Done, C., Johnson, W. N., Ebisawa, K., Ueda, Y., Haardt, F., Philips, B. F. 1997, MNRAS, 288, 958
- Grabelsky et al. 1993 BAAS, 183<sup>th</sup> AAS meeting, 25, 1337
- Grebenev et al. 1993 A&AS, 97, 281
- Grove, J. E. 1999, in ASP Conf. Ser. 161, High Energy Processes in Accreting Black Hole, ed. J. Poutanen & R. Svensson. (San Francisco: ASP), 54
- Homan J., Buxton, M., Markoff, S., Bailyn., C. D., Nespoli, E. et Belloni, T., 2005, ApJ, 624, 295
- Hynes, R. I., Steeghs, D., Casares, J., Charles, P. A., & O'Brien, K. 2003, ApJ, 583, L95
- Jensen, P. L., Clausen, K., Cassi, C., Ravera, F., Janin, G., Winkler, C., & Much, R. 2003, A&A, 411, 7
- Johnson, W. N., et al. 1993, A&AS, 97, 21
- Kalemci, E., Tomsick, J. A., Buxton, M. M., Rothschild, R. E., Pottschmidt, K., Corbel, S., Brocksopp, C. & Kaaret, P. 2005, ApJ, 622, 508
- Kalemci, E., Tomsick, J. A., Rothschild, R. E., Pottschmidt, K., Corbel, S. & Kaaret, P. 2006, ApJ, 639, 340
- Kong, A. K. H., Charles, P. A., Kuulkers, E., & Kitamoto, S. 2002, MNRAS, 329, 588
- Kuulkers, E., et al. 2004, Astron. Tel., 240
- Lebrun, F., et al. 2003, A&A, 411, L141



- Ling, J. C., Wheaton, Wm. A., Skelton, R. T., Harmon, B. A., Rubin, B. C., Fishman, G. J., & Paciesas, W. S. 1994, BAAS, 184<sup>th</sup> AAS meeting, 26, 971
- Magdziarz, P., & Zdziarski, A. A. 1995, MNRAS, 273, 837
- Markert, T. H., Canizares, C. R., Clark, G. W., Lewin, W. H. G., Schnopper, H. W., & Sprott, G. F. 1973, ApJ, 84, 67
- Malzac, J., et al. 2006, A&A, 448, 1125
- Markoff, S., Nowak, M., Corbel, S., Fender, R. & Falcke, H. 2003, A&A, 397, 645
- McClintock, J.E., & Remillard, R.A. 2006, in Compact Stellar X-ray Sources, ed. W.H.G. Lewin & M. van der Klis (Cambridge: Cambridge University Press), p157 astro-ph/0306213.
- McClintock, J.E., et al., 2001, ApJ, 555, 477
- McConnell, M. L., et al. 2000, ApJ, 543, 928
- Miller, J. M., et al. 2004a, ApJ, 601, 450
- Miller, J. M., et al. 2004b, ApJ, 606, L131
- Miller, J. M., Homan, J., Steeghs, D., Rupen, M. Hunstead, R. W., Wijnands, R., Charles, P. A., & Fabian, A. C. 2006, ApJ, in press (astro-ph/0602633)
- Nowak, M.A., Wilms, J., & Dove, J.B. 2002, MNRAS, 332, 856
- Poutanen, J., & Svensson, R. 1996, ApJ, 470, 249
- Remillard, R. A. 2005, Procs. 22nd Texas meeting on Relativistic Astrophysics, Stanford University, astro-ph/0504129
- Revnivtsev, M., Gilfanov, M., & Churazov, E. 2001, A&A, 380, 520
- Rodriguez, J., et al. 2006, MNRAS, 366, 274
- Roques, J. P., et al. 2003, A&A, 411, L91
- Rothschild, R. E., et al. 1998, ApJ, 496, 538
- Shahbaz, T., Fender, R., & Charles, P. A. 2001, A&A, 376, L17
- Skinner, G., & Connell, P. 2003, A&A, 411, L123

- Smith, D. M., Heindl, W. A., Swank, J. H., Wilms, J. & Pottschmidt, K. 2004, *Astron. Tel.*, 231
- Sturmer, S. J., et al. 2003, *A&A*, 411, L81
- Tomsick, J. A., Corbel, S. & Kaaret, P. 2001, *ApJ*, 563, 229
- Vedrenne, G., et al. 2003, *A&A*, 411, L63
- Wardzinski, G., Zdziarski, A. A., Gierliński, M., Grove, J. E., Jahoda K., & Johnson, W., N. 2002, *MNRAS*, 337, 829
- Zdziarski, A. A., Lubinski, P., & Smith, D. A. 1999, *MNRAS*, 303, L11
- Zdziarski, A. A., Lubiński, P., Gilfanov, M., & Revnivtsev, M. 2003, *MNRAS*, 342, 355
- Zdziarski, A. A., Gierliński, M., Mikolajewska, J., Wardzinski, G., Smith, D. M., Alan, H. B. & Kitamoto, S., 2004, *MNRAS* 351, 791

Rev.	INT <sub>start</sub>	INT <sub>stop</sub>	$\Delta t_{sp}$ (ks)	ID	RX <sub>start</sub>	RX <sub>stop</sub>	Exp.(ks)
166	53057.07	53059.45	152	90109-01-01-00	53058.99	53059.17	16.1
167	53061.62	53062.22	40	80132-01-07-00	53061.75	53061.86	9.3
174	53080.99	53081.67	38	90118-01-06-00	53081.51	53081.54	2.8
175	53084.77	53085.45	43	80102-04-66-00	53084.46	53084.49	2.5

Table 1: The INTEGRAL observations of GX 339-4. For each INTEGRAL revolution (Rev.), we give the beginning INT<sub>start</sub> and the end INT<sub>stop</sub> of the INTEGRAL observations in MJD.  $\Delta t_{sp}$  is the useful duration for SPI observations. ID is the identification program number of RXTE observations. RX<sub>start</sub> and RX<sub>stop</sub> are the beginning and the end of RXTE observations taken (quasi-) simultaneously with INTEGRAL observations. Exp. is the exposure time for PCA.

Source	$\Phi$ (23-50)	$\sigma$ (23-50)	$\sigma$ (50-95)	$\sigma$ (95-195)
4U 1700-377	233.5 ± 6.1	38.3	11.9	5.3
4U 1630-47	85.6 ± 2.1	40.1	10.6	7.5
GX 339-4	44.2 ± 2.3	19.6	10.5	8.5
IGR J16316-4028	21.9 ± 2.8	7.9	-	-
OA0 1657-415	26.7 ± 1.9	13.6	-	-
4U 1636-536	44.4 ± 2.5	17.6	-	-
H 1705-440	68.2 ± 2.2	31.0	-	-
GX 354-0	150.2 ± 5.8	25.9	6.6	-
GX 340+0	31.3 ± 2.1	14.9	-	-
1E 1740.7-2942	62.6 ± 15.9	3.9	2.2	2.2
4U 1625-33	27.5 ± 4.4	6.3	2.9	2.2

Table 2: Sources detected by SPI in the field of view of GX 339-4 during revolution 166+167:  $\Phi$  is the flux in the 23-50 keV energy range and  $\sigma$ , the significance in the 23-50 keV, 50-95 keV and 95-195 keV energy ranges.

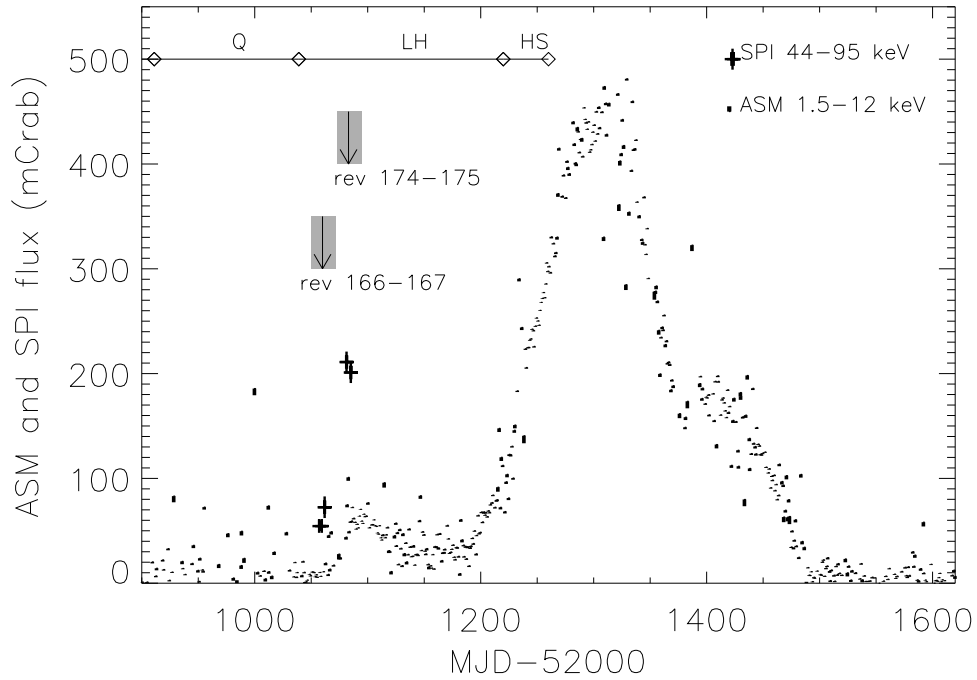


Fig. 1.— *RXTE* ASM and SPI light curves of GX 339-4 showing a quiescent period followed by the 2004 outburst. The different states harboured by the source are summarized on the graph : Q=quiescent, LH=low/hard and HS=high/soft (see Remillard 2005). The arrows represent the *INTEGRAL* observation periods (revolutions 166, 167, 174 and 175).

Revolution	$\Phi_{23-44}$	$\Phi_{44-95}$
166+167	$42 \pm 2$	$59 \pm 4$
174	$156 \pm 6$	$211 \pm 10$
175	$152 \pm 6$	$201 \pm 10$

Table 3: Flux of GX 339-4 observed by SPI, for datasets introduced in Table 1, in the 23-44 keV and 44-95 keV energy ranges (expressed in mCrab).

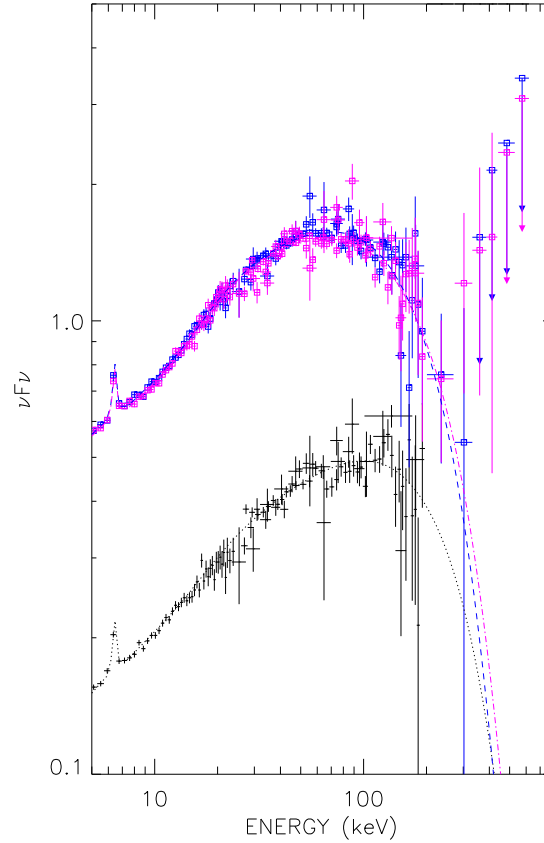


Fig. 2.— Deconvolved spectra of GX 339-4 with simultaneous PCA (3.-25 keV), HEXTE (25-200 keV), SPI (23-600 keV) and ISGRI (25-518 keV) data, for revolutions 166+167 (black points), 174 (blue squares) and 175 (magenta squares). The lines correspond to the best fits with the EQPAIR thermal model (see table 6).

rev	$\Gamma$	$E_c$ keV	$\Omega/2\pi$	$W_{Fe}$ eV	$\chi^2(\text{dof})$	F-test
166+167	$1.58^{+0.02}_{-0.02}$	$365^{+100}_{-67}$	$0.22^{+0.06}_{-0.06}$	$88^{+33}_{-29}$	0.82(172)	
166+167	$1.65^{+0.01}_{-0.01}$	2000 (fr)	$0.35^{+0.05}_{-0.05}$	$79^{+35}_{-30}$	1.10(173)	$1.0 \times 10^{-12}$
174	$1.64^{+0.02}_{-0.02}$	$293^{+60}_{-41}$	$0.43^{+0.08}_{-0.07}$	$94^{+43}_{-36}$	0.91(114)	
174	$1.77^{+0.01}_{-0.01}$	2000 (fr)	$0.80^{+0.06}_{-0.07}$	$94^{+34}_{-34}$	1.68(115)	$2.7 \times 10^{-17}$
175	$1.67^{+0.02}_{-0.02}$	$325^{+68}_{-50}$	$0.50^{+0.08}_{-0.07}$	$77^{+38}_{-36}$	1.09(100)	
175	$1.78^{+0.01}_{-0.01}$	2000 (fr)	$0.85^{+0.07}_{-0.07}$	$82^{+40}_{-41}$	1.78(101)	$1.53 \times 10^{-12}$
175*	$1.69^{+0.02}_{-0.02}$	$402^{+103}_{-71}$	$0.52^{+0.08}_{-0.08}$	$77^{+38}_{-36}$	1.60(114)	
175*	$1.79^{+0.01}_{-0.01}$	2000 (fr)	$0.82^{+0.06}_{-0.05}$	$72^{+34}_{-36}$	2.02(115)	$1.94 \times 10^{-7}$

Table 4: PCA, HEXTE, SPI and ISGRI data fitted simultaneously using the XSPEC multicomponent model PHABS\*(PEXRAV+GAUSSIAN).  $\Gamma$  is the photon index and  $E_c$  the energy cut-off. Gaussian line was fixed at an energy of 6.4 keV with a width fixed to 0.1 keV.  $W_{Fe}$  is the equivalent width.  $\Omega/2\pi$  is the reflection fraction. The F-test is calculated between models with free cut-off and no (ie fixed) cut-off. We show for the dataset of revolution 175, the fit parameters in the case for which the HEXTE data have been included (175\*).

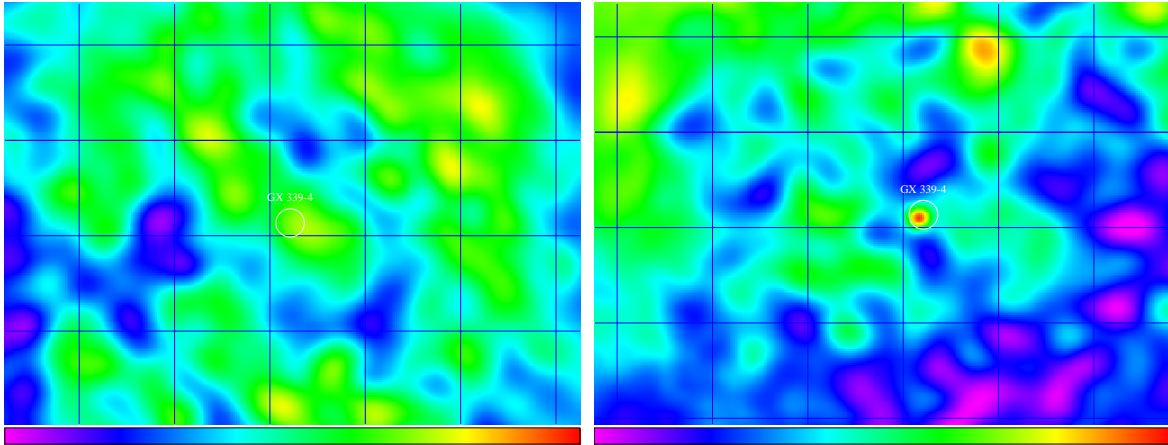


Fig. 3.— Significance maps obtained with SPIROS in the 200-437 keV energy range; the color scale is from  $-3\sigma$  to  $4.5\sigma$ ; grid spacing is  $5^\circ$ . Left: revolution 174, the significance of the GX 339-4 flux is below  $1.5\sigma$ . Right: revolution 175, GX 339-4 is the only significant source of the field of view detected with a flux of  $193.4 \pm 46.6$  mCrab ( $4.2\sigma$ ).

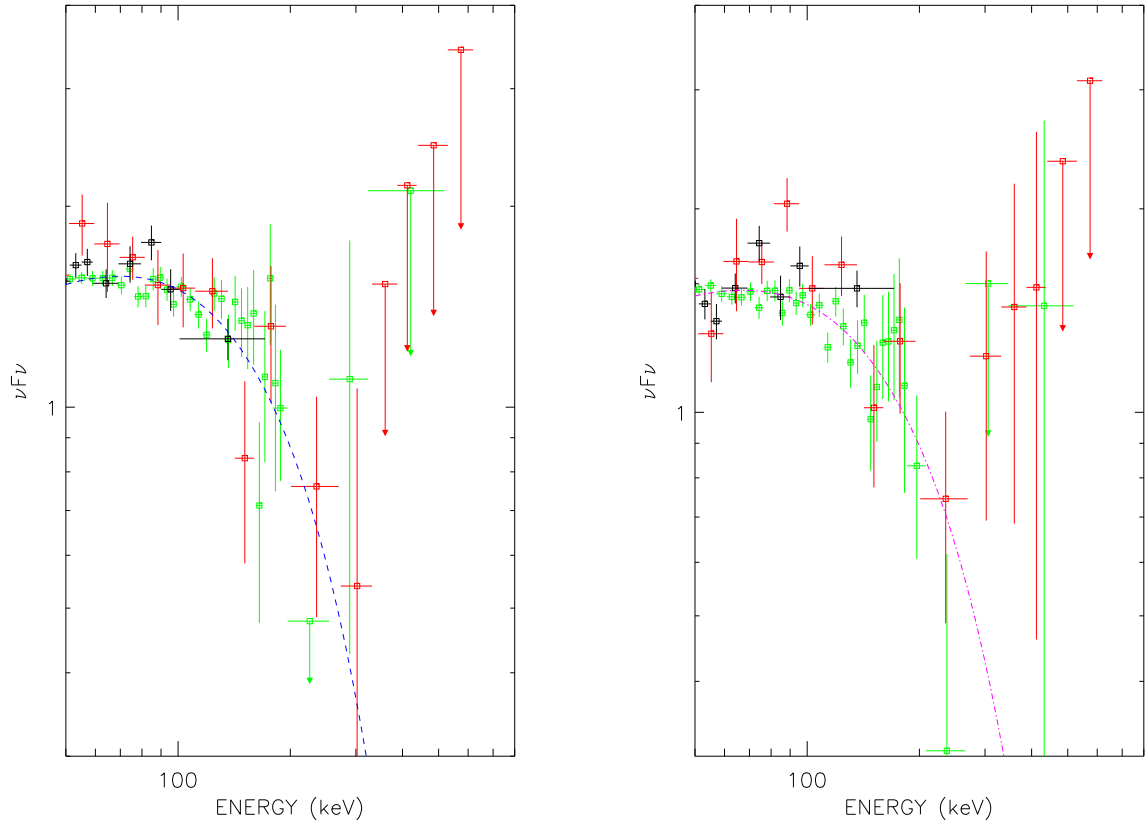


Fig. 4.— High energy part of the GX 339-4 deconvolved spectra for revolution 174 (left) and for revolution 175 (right) with HEXTE (black points), SPI (red points) and ISGRI (green points) data. The line corresponds to the best fit with the EQPAIR thermal model (see table 6).

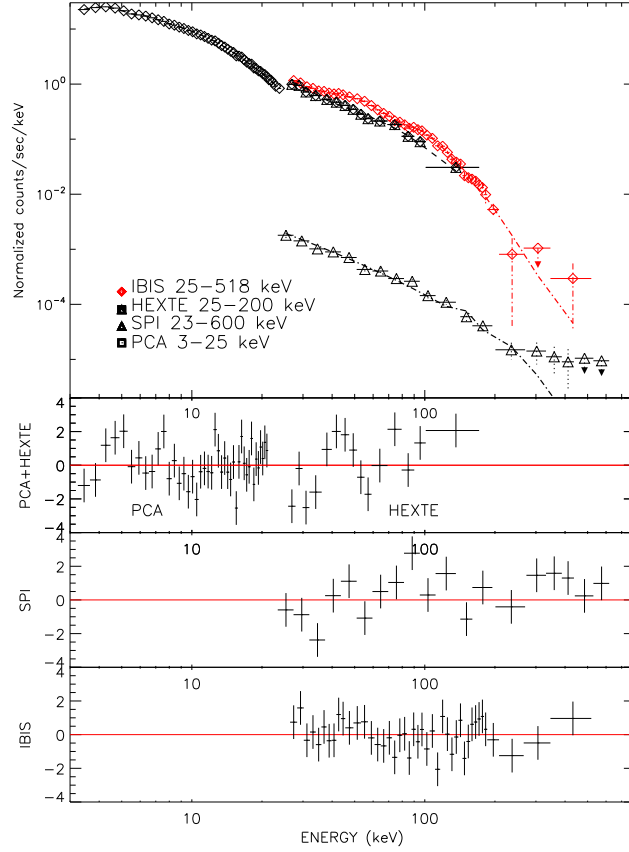


Fig. 5.— Spectra of GX 339-4 with simultaneous PCA, HEXTE, ISGRI and SPI data for revolution 175. The COMPSS model used is described in Table 5. The residuals obtained for each instrument are presented in the bottom panels.

rev	kT keV	$\tau$	$W_{Fe}$ keV	$\Omega/2\pi$	$L_{2-600}$ $\times 10^{36} \text{ erg s}^{-1}$	y	$\chi^2(\text{dof})$
166+167	$72^{+21}_{-18}$	$2.40^{+0.72}_{-0.64}$	$87^{+28}_{-46}$	$0.23^{+0.06}_{-0.06}$	$12.8^{+1.0}_{-1.0}$	1.35	0.88(172)
174	$64^{+10}_{-7}$	$2.43^{+0.48}_{-0.53}$	$91^{+31}_{-40}$	$0.37^{+0.06}_{-0.05}$	$35.5^{+0.1}_{-0.2}$	1.22	0.82(113)
175	$61^{+12}_{-8}$	$2.54^{+0.46}_{-0.48}$	$90^{+30}_{-34}$	$0.43^{+0.06}_{-0.06}$	$34.9^{+0.1}_{-0.3}$	1.22	1.28(98)
175*	$59^{+11}_{-7}$	$2.64^{+0.44}_{-0.46}$	$91^{+37}_{-35}$	$0.41^{+0.06}_{-0.06}$	$34.9^{+0.1}_{-0.3}$	1.22	1.46(113)

Table 5: PCA, HEXTE, SPI and ISGRI data fitted simultaneously using the XSPEC multi-component model PHABS\*(COMPSS+GAUSSIAN). Gaussian line was fixed at an energy of 6.4 keV with a width fixed to 0.1 keV. The seed photon temperature  $kT_{seed}$  was frozen to 390 eV.  $W_{Fe}$  is the equivalent width.  $\Omega/2\pi$  is the reflection fraction.  $L_{2-600}$  is the luminosity of the source in the 2-600 keV energy range. We show for the dataset of revolution 175, the fit parameters in the case for which the HEXTE data have been included (175\*).



rev	$l_h/l_s$	$l_{nth}/l_{th}$	$\tau_{es}$	$W_{Fe}$ eV	$\Omega/2\pi$	$\tau_{tot}$	kT keV	y	$\chi^2(\text{dof})$
166+167	$5.74^{+0.19}_{-0.32}$	0 fr	$1.15^{+0.05}_{-0.11}$	$77^{+30}_{-40}$	$0.30^{+0.03}_{-0.04}$	1.15	98	0.88	0.94(173)
166+167	$6.32^{+0.10}_{-0.10}$	0 fr	1.60 fr	$83^{+50}_{-46}$	$0.26^{+0.03}_{-0.03}$	1.60	72	0.90	0.98(174)
174	$5.08^{+0.17}_{-0.12}$	0 fr	$1.61^{+0.08}_{-0.07}$	$97^{+50}_{-35}$	$0.42^{+0.03}_{-0.03}$	1.61	64	0.81	0.82(114)
174	$6.35^{+0.88}_{-1.11}$	$0.40^{+0.3}_{-0.3}$	$1.98^{+0.14}_{-0.18}$	$102^{+50}_{-50}$	$0.39^{+0.04}_{-0.04}$	2.00	50	0.78	0.82(113)
175	$5.09^{+0.13}_{-0.05}$	0 fr	$1.66^{+0.06}_{-0.03}$	$90^{+30}_{-50}$	$0.43^{+0.03}_{-0.03}$	1.60	64	0.80	1.10(99)
175	$5.61^{+2.15}_{-0.16}$	$0.28^{+0.45}_{-0.17}$	$1.54^{+0.49}_{-0.12}$	$90^{+30}_{-50}$	$0.47^{+0.05}_{-0.06}$	1.56	64	0.78	1.06(98)
175*	$5.08^{+0.17}_{-0.12}$	0 fr	$1.61^{+0.07}_{-0.02}$	$90^{+36}_{-50}$	$0.42^{+0.03}_{-0.04}$	1.61	64	0.81	1.47(114)
175*	$7.08^{+0.46}_{-0.42}$	$0.65^{+0.17}_{-0.14}$	$1.92^{+0.15}_{-0.07}$	$94^{+92}_{-59}$	$0.45^{+0.06}_{-0.05}$	1.93	50	0.76	1.45(113)

Table 6: PCA, HEXTE, SPI and ISGRI data fitted simultaneously using EQPAIR model combined with a Gaussian iron line. See text for the parameters description.  $kT_{seed}$  has been frozen to 390 eV, with an inclination angle of 50 degrees.  $\tau_{tot}$  and kT are calculated from fitted parameters. We show for the dataset of revolution 175, the fit parameters in the case for which the HEXTE data have been included (175\*).